MOLECULAR PHYSICS e2267135
https://doi.org/10.1080/00268976.2023.2267135

Taylor & Francis
Taylor & Francis Group

RESEARCH ARTICLE



# A computational and spectroscopic study of MgCCH ($X^2\Sigma^+$): towards characterizing $MgCCH^+$

Joseph E. Burns[a], Qianyi Cheng[a], Ryan C. Fortenberry [b], Ming Sun[c], Lindsay N. Zack[c], Trishal Zaveri[c], Nathan J. DeYonker[a] and Lucy M. Ziurys[c]

[a]Department of Chemistry, University of Memphis, Memphis, TN, USA; [b]Department of Chemistry and Biochemistry, University of Mississippi, Oxford, MS, USA; [c]Departments of Astronomy and Chemistry, Arizona Radio Observatory, and Steward Observatory, University of Arizona, Tucson, AZ, USA

**ABSTRACT**

New computational and experimental studies have been carried out for the MgCCH radical in its $X^2\Sigma^+$ state. Coupled cluster theory [CCSD(T)], was used in conjunction with post-CCSD(T) and scalar relativistic additive corrections to compute vibrational quartic force fields for MgCCH and its cation. From the quartic force fields, higher-order spectroscopic properties, including rotational constants, were obtained. In tandem, the five lowest energy rotational transitions for MgCCH, $N = 1 \rightarrow 0$ through $N = 5 \rightarrow 4$, were measured for the first time using Fourier transform microwave/millimetre wave methods in the frequency range 9–50 GHz. The radical was created in the Discharge Assisted Laser Ablation Source (DALAS) developed in the Ziurys group. A combined fit of these data with previous millimetre direct absorption measurements have yielded the most accurate rotational constants for MgCCH to date. The computed principle rotational constant lies within ~ 1.51–1.65 MHz of the experimental one, validating the computational approach. High-level theory was then applied to produce rovibrational spectroscopic constants for $MgCCH^+$, including a rotational constant of $B_0 = 5354.5$–5359.5 MHz. These new predictions will further the experimental study of $MgCCH^+$, and aid in the low-temperature characterisation of MgCCH in the interstellar medium.

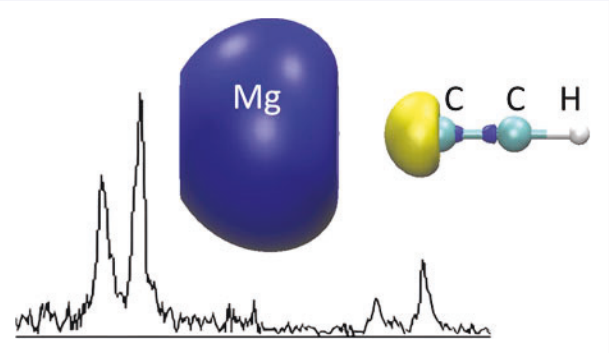


**ARTICLE HISTORY**
Received 13 August 2023
Accepted 29 September 2023

**KEYWORDS**
Magnesium free radicals; rotational spectroscopy; quartic force fields; astrochemistry; computational chemistry

## Q1 Introduction

The Interstellar Medium (ISM) contains many terrestrial and non-terrestrial compounds [1,2] including those with metals such as sodium, aluminum, potassium, vanadium and iron [3]. However, recent observations of interstellar molecules have strongly focused on magnesium. A slew of Mg-bearing carbon chains have now been identified in the interstellar gas, such as MgCN, $MgC_3N$, $MgC_5N$, $MgC_4H$, $MgC_6H$, and $MgC_4H^+$ [4–6] among several others [7]. Remarkably, these species have been identified almost entirely in the circumstellar envelope of the carbon star IRC + 10216 [8]; MgNC has also been detected in the protoplanetary nebulae CRL2688 and CRL618 [9]. However, to date there have been no observations of a Mg-bearing molecule in molecular clouds, suggesting that dust condensation plays an important role in magnesium chemistry. Note that magnesium is depleted by about a factor of 10 in diffuse clouds.

**CONTACT** Nathan J. DeYonker ndyonker@memphis.edu Department of Chemistry, University of Memphis, Memphis, TN 38152, USA

Supplemental data for this article can be accessed online at https://doi.org/10.1080/00268976.2023.2267135.

Magnesium is a common crystalline material found in the Earth's crust and mantle and is found to be more abundant in the spectra of stars which host planets [10], suggesting it might play a role in planet formation buildup from dust grains.

As such, several questions surround the role that element 12 plays in various astrochemical regions. Do magnesium-containing molecules dominate the inorganic inventory of the known inorganic/organometallic astrochemicals because they are the most common/abundant? Or have magnesium-bearing molecules be come a prominent target for astrochemists and spectroscopists because they mostly lack the multireference issues and spectral perturbations that plague characterisation and observation of transition-metal containing molecules? Nevertheless, understanding the synthesis of these molecules and how they relate to the presence of magnesium in the solid state remains a challenge for the astrochemistry community, as it also can for other disciplines that employ this element such as materials science or alternative fuels.

More Mg-bearing molecules are likely to be discovered in the ISM, but synthesising and measuring laboratory spectra of such species is difficult. Many of the possible compounds are radicals and ions, which are always challenging to create in detectable quantities in the laboratory. Computational modelling of small magnesium-bearing species is, therefore, essential. Not only does quantum chemistry provide structures and estimates of spectroscopic constants for experimentalists, but also serves as a source of other molecular properties crucial for astrochemical modelling, such as line strengths and transition moments.

Magnesium acetylide and its cation ($MgCCH^{0/1+}$) are excellent candidates for interstellar identification. The presence of magnesium-containing molecules in the envelope of IRC + 10216 [4], as well as the high abundance of CCH, suggests the presence of both MgCCH and $MgCCH^+$ in this famous source. Indeed, Cernicharo and co-authors have tentatively detected MgCCH in IRC + 10216 [11]. These studies were based on laboratory spectroscopy studies of Ziurys and co-workers, as detailed below [12,13]. The astrochemical detection of MgCCH, however, has been difficult to confirm due to line contamination and the intrinsic weakness of spectral features. However, an updated study by the Cernicharo group provides several more rotational lines for MgCCH [5] giving stronger evidence for its inclusion in interstellar molecular censuses. Somewhat surprisingly, though, experimental data on the related cation, $MgCCH^+$, does not currently exist.

The first experimental measurements of MgCCH occurred in 1995, when Anderson and Ziurys recorded the millimetre-wave spectrum of the radical in the laboratory. They found the molecules to be linear with a $^2\Sigma^+$ ground electronic state [12]. The molecule was synthesised by the reaction of magnesium vapour with acetylene seeded in argon in a DC discharge. Additional rotational spectra of MgCCH were later recorded by Brewster, Ziurys, and coworkers for both the vibrational ground state and vibrational satellite lines of the Mg-C–C bending mode ($\nu_5$) using millimetre-wave direct absorption techniques [13]. Further studies of this molecule include the first laser-induced fluorescence (LIF) spectrum of the $A^2\Pi$-$X^2\Sigma$ electronic transition of MgCCH, which assigned the Mg-C stretching mode [14] as well as high-resolution laser spectroscopy of this transition using a novel molecular beam source [15]. Thompson and Andrews also investigated reactions of laser-ablated magnesium atoms with acetylene in argon matrices to gather infrared absorption spectra for the products [16]. In addition to these experiments, previous computational work on this molecule characterised vibrational spectra with coupled cluster theory [17], as well as a CASPT2 study that included MgCCH in an analysis of magnesium-containing carbon chains [18]. Furthermore, reaction pathways for MgCCH formation was also explored theoretically [19], but poor overlap between quantum chemistry and experiment has led to a notable amount of uncertainty in various molecular properties.

Quantum chemistry is a powerful tool for astrochemical application in computing gas phase spectral data for elucidating and validating experimental results. In this work, quartic force fields (QFF) and high-level electronic structure theories are utilised to generate accurate rovibrational spectroscopic data [20]. The QFF is an energy surface representing a fourth-order Taylor series expansion for the potential of the internuclear Hamiltonian and takes the form of:

$$V = \frac{1}{2}\sum_{ij} F_{ij}\Delta_i\Delta_j + \frac{1}{6}\sum_{ijk} F_{ijk}\Delta_i\Delta_j\Delta_k + \frac{1}{24}\sum_{ijkl} F_{ijkl}\Delta_i\Delta_j\Delta_k\Delta_l \quad (1)$$

where $\Delta_{ij\ldots}$ are displacements along normal coordinates and $F_{ij}\ldots$ are the force constants of the same unrestricted indices. Treating the QFF with second-order vibrational perturbation theory [21–23] (VPT2) has produced vibrational frequencies within 1.0 $cm^{-1}$ as well as rotational constants within 30 MHz of experiment for gas phase organic polyatomic molecules [24,25]. Recently, DeYonker, Fortenberry, and Cheng have modified the black box, coupled cluster QFF approach pioneered by Lee, Fortenberry, and Huang to study inorganic vibrational spectroscopy [26,27]. The approach has been successfully

used to explore neutral molecules and cations containing magnesium [28]. These same types of computations will be utilised here for MgCCH to provide a more complete description of MgCCH/$MgCCH^+$ rovibrational properties.

In addition, pure rotational spectra of MgCCH in its ground electronic state were recorded in the frequency range 9–50 GHz using Fourier transform microwave/millimetre-wave (FTMmmW) techniques. These data complement the previous mm-wave direct absorption measurements and improve the overall accuracy of the rotational constants. Furthermore, the proton hyperfine constants of MgCCH have been established for the first time. Vibration-less rotational line lists of MgCCH were then constructed, purely from the theoretical VPT2 spectroscopic constants, and show remarkable agreement with experiment.

## Experimental methods

The FTMmmW spectrometer of the Ziurys group was used to measure the rotational spectrum of the MgCCH radical ($X^2\Sigma^+$). This instrument is described in detail elsewhere [29]. Briefly, this Balle-Flygare spectrometer comprises a Fabry–Perot cavity with two spherical aluminum mirrors in a near confocal arrangement housed in a cryo-pumped vacuum chamber. Two sets of mirrors are used to cover the range 4–40 GHz and 40–90 GHz. Each mirror has an embedded antenna ( $<40$ GHz) or waveguide ( $>40$ GHz) to either transmit or receive the microwave radiation. Molecules are injected into the cavity via a pulsed nozzle oriented 40° with respect to the optical axis, and the resulting molecular beam supersonically expands into the chamber. Radiation at a given frequency is then introduced as a short pulse into the cavity, which supports a $\sim$1 MHz instantaneous bandwidth. The radiation is absorbed by the molecules in the beam if there is a resonant transition; their subsequent emission signal is then collected by a low noise amplifier (LNA) as a function of time, the so-called 'free induction decay', or FID. The time-domain signals are fast-Fourier-transformed to create spectra with 2 kHz resolution. Each transition appears as a Doppler doublet, with the transition frequency being the average of the two doublets.

MgCCH was synthesised using the Discharge Assisted Laser Ablation Source (DALAS), first developed in the Ziurys group [30]. This source combines a typical laser ablation source with a DC discharge at the exit port. The rotating/translating magnesium rod (ESPI metals) was ablated using a Nd:YAG laser (Continuum Surelite I-10), and the metal vapour entrained in a 0.1% acetylene in argon mixture supercooled in the nozzle. The DC discharge was operated at $\sim$ 10 volts.

## Computational details

All computations employed the MOLPRO2018 software package [31]. Geometry optimizations occurred at the coupled cluster singles, doubles and perturbative triples [CCSD(T)] [32] and explicitly-correlated coupled cluster [CCSD(T)-F12] [33] levels of theory across multiple basis sets. Correlation consistent basis sets were used [34] that include diffuse functions (aug-cc-pVDZ to aug-cc-pV5Z), optimised contractions to incorporate the 2nd-order Douglas-Kroll [35] Hamiltonian to account for scalar relativistic effects (aug-cc-pVDZ-DK to aug-cc-pV5Z-DK), tight functions to account for core-valence correlation (cc-pwCVQZ-DK), and correlation consistent basis sets optimised for explicitly correlated coupled cluster theory [36] (cc-pVDZ-F12, cc-pVTZ-F12, cc-pwCVTZ-F12, cc-pVQZ-F12). Reference internal coordinate parameters for our vibrational force field calculations were defined by:

$$r_{cc-pVQZ-F12} + (r_{cc-pwCVTZ-F12} - r_{cc-pCVTZ-F12-\mathrm{valence}}) \quad (2)$$

In the QFF computations, positive and negative displacements were calculated from Equation (2) up to the fourth-order in increments of 0.005 radians for bond angles and 0.005 Å for bond lengths. The QFF required 625 single point energies using the following symmetry-internal coordinates:

$$S_1(\Sigma^+) = Mg - C$$

$$S_2(\Sigma^+) = C - C$$

$$S_3(\Sigma^+) = C - H$$

$$S_4(\Pi_{xz}) = \angle Mg - C - C - y$$

$$S_5(\Pi_{xz}) = \angle C - C - H - y$$

$$S_6(\Pi_{yz}) = \angle Mg - C - C - x$$

$$S_7(\Pi_{yz}) = \angle C - C - H - x$$

where $S_4$–$S_7$ represents linear out-of-plane bends which are perpendicular to the $x$ and $y$ axes.

Both CCSD(T) and CCSD(T)-F12 levels of theory were utilised as well as multiple basis sets in the construction of the QFF via the 'CcC' approach of Lee, Fortenberry, and Huang, and coworkers [24]. This included a complete basis set extrapolation, 'C', and consideration of core-valence electron correlation, 'cC'. The CcC energies are computed at each point on the grid using aug-cc-pVQZ (aVQZ), aug-cc-pV5Z (aV5Z), and cc-pwCVQZ

(wCVQZ) basis sets. The aVQZ-DK and aV5Z-DK energies at each point are extrapolated to the one-electron complete basis set (CBS) via a two-point formula,

$$E(l) = E(CBS) + A(l_{max} + 1/2)^{-4}. \quad (3)$$

The core-valence correction is computed via

$$E(CV) = E_{CCSD(T)\ wCVQZ} - E_{CCSD(T)\ wCVQZ-\text{valence}}. \quad (4)$$

In the CV computations with correlated outer core molecular orbitals, the Mg 1 s orbital is still frozen.

Extra considerations in the pursuit of improving accuracy for inorganic molecules included scalar relativistic corrections as well as post-CCSD(T) calculations [26]. In the current study, these additive corrections are a small basis set CCSDT correction as well as a small basis set scalar relativistic correction,

$$\Delta(CCSDT) = E_{CCSDT\ aVDZ-DK} - E_{CCSD(T)\ aVDZ-DK} \quad (5)$$

and

$$\Delta(DK) = E_{CCSD(T)-DK\ aVDZ-DK} - E_{CCSD(T)\ aVDZ}. \quad (6)$$

In addition to the 'CcC' terminology, the Δ(CCSDT) correction adds an 'E' term to the named composite approaches for higher-order electron correlation (CcCE) and the Δ(DK) adds an 'R' for relativistic effects (CcCR, and CcCRE when both additive corrections are included). Similarly, a CcC-F12 approach was tested, where the CcC energy is defined as

$$E(CcC-F12) = E_{cc-pVQZ-F12} + (E_{cc-pwCVTZ-F12} - E_{cc-pCVTZ-F12-\text{valence}}). \quad (7)$$

A least-squares fit identifies the minimum QFF equilibrium geometry; the sum of squared residuals for each fitting is on the order of $10^{-17}$ (a.u.)$^2$ or better. At the minimum, a refitting of the QFF surface generates force constants and the equilibrium geometry at a given level of theory. The INTDER [37] programme transforms the force constants from symmetry-internal to Cartesian coordinates. This is fed into SPECTRO [38] package which produces anharmonic frequencies as well as higher order spectroscopic constants with VPT2. The PGOPHER [39] programme uses these constants to simulate the rotational spectrum from theoretical constants at 15 K, the temperature for the astrophysical region of interest.

## Results and discussion

### New FTMmmW measurements for MgCCH

The new rotational transitions measured for MgCCH ($X^2\Sigma^+$) are presented in Table 1. Note that $\nu_{calc}$ in Table 1 refers to rotational transitions obtained from the fitted experimental Hamiltonian, not from quantum chemical computations. As shown, five transitions were recorded successively from the $N = 1 \rightarrow 0$ line near 10 GHz through the $N = 5 \rightarrow 4$ line at 49 GHz. Each rotational transition $N+1 \rightarrow N$ is split into spin-rotation doublets, indicated by quantum number $J$. In addition, each

**Table 1.** Observed rotational transitions of MgCCH($\tilde{X}^2\Sigma^+$)[a].

| $N'$ | $J'$ | $F'$ | → | $N''$ | $J''$ | $F''$ | $\nu_{obs}$ | $\nu_{obs}$-$\nu_{calc}$ |
|---|---|---|---|---|---|---|---|---|
| 1 | 0.5 | 0 | → | 0 | 0.5 | 1 | 9913.391 | 0.0048 |
| 1 | 0.5 | 1 | → | 0 | 0.5 | 0 | 9917.113 | 0.0061 |
| 1 | 1.5 | 1 | → | 0 | 0.5 | 1 | 9936.195 | 0.0054 |
| 1 | 1.5 | 2 | → | 0 | 0.5 | 1 | 9938.931 | −0.00078 |
| 1 | 1.5 | 1 | → | 0 | 0.5 | 0 | 9940.903 | −0.00105 |
| 2 | 1.5 | 2 | → | 1 | 0.5 | 1 | 19852.696 | 0.00372 |
| 2 | 1.5 | 1 | → | 1 | 0.5 | 0 | 19853.248 | 0.00464 |
| 2 | 2.5 | 3 | → | 1 | 1.5 | 2 | 19869.574 | −0.00030 |
| 2 | 2.5 | 2 | → | 1 | 1.5 | 1 | 19869.850 | 0.00429 |
| 3 | 2.5 | 3 | → | 2 | 1.5 | 2 | 29783.341 | 0.00488 |
| 3 | 2.5 | 2 | → | 2 | 1.5 | 1 | 29783.502 | 0.00257 |
| 3 | 3.5 | 4 | → | 2 | 2.5 | 3 | 29800.086 | −0.0025 |
| 3 | 3.5 | 3 | → | 2 | 2.5 | 2 | 29800.209 | 0.00605 |
| 4 | 3.5 | 4 | → | 3 | 2.5 | 3 | 39713.730 | 0.00787 |
| 4 | 3.5 | 3 | → | 3 | 2.5 | 2 | 39713.801 | −0.00360 |
| 4 | 4.5 | 5 | → | 3 | 3.5 | 4 | 39730.437 | 0.00600 |
| 4 | 4.5 | 4 | → | 3 | 3.5 | 3 | 39730.488 | −0.00853 |
| 5 | 4.5 | 5 | → | 4 | 3.5 | 4 | 49643.870 | 0.00138 |
| 5 | 4.5 | 4 | → | 4 | 3.5 | 3 | 49643.870 | −0.04885 |
| 5 | 5.5 | 6 | → | 4 | 4.5 | 5 | 49660.556 | −0.00290 |
| 5 | 5.5 | 5 | → | 4 | 4.5 | 4 | 49660.611 | 0.01002 |

[a]In MHz.

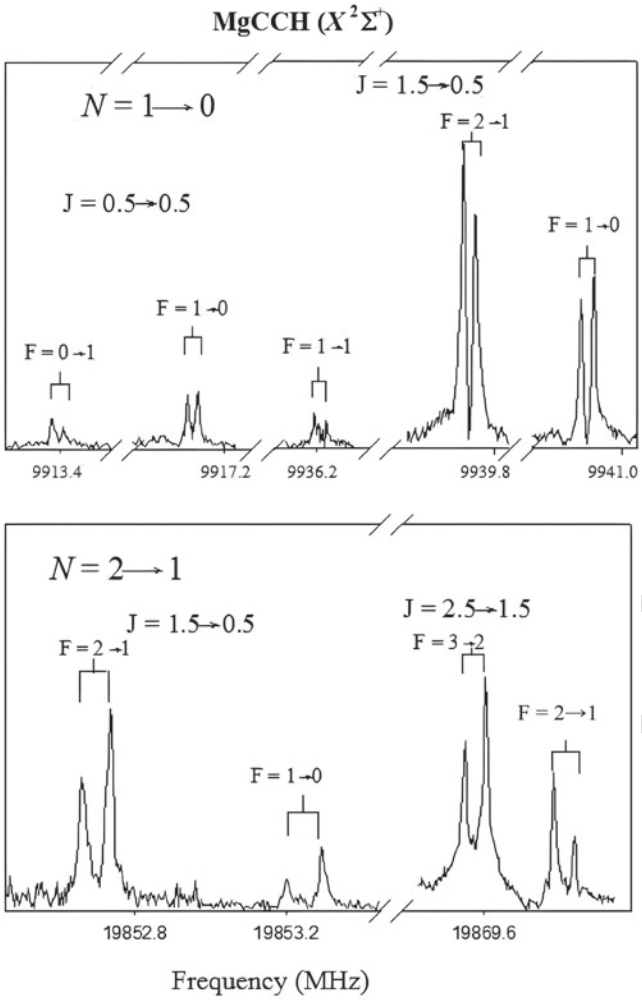


**Figure 1.** FTMmmW spectra of MgCCH ($X^2\Sigma^+$) displaying the N = 1 → 0 and N = 2→ 1 transitions near 10 and 20 GHz, respectively. Each spectrum is split into doublets by spin-rotation coupling, labelled by quantum number *J*. Proton hyperfine interactions further split the spectra into multiple lines, indicated by *F*, where $\boldsymbol{F} = \boldsymbol{J} + \boldsymbol{I}$. The Doppler doublets are indicated by brackets. There are frequency breaks in the spectra to show multiple hyperfine features.

spin-rotation doublet is affected by hyperfine interactions arising from the nuclear spin of the proton, $I = \frac{1}{2}$, which further splits the lines. The hyperfine components are labelled by quantum number *F*, where $\boldsymbol{I} + \boldsymbol{J} = \boldsymbol{F}$ in a Hund's case $b_{\beta J}$ basis.

Representative spectra for MgCCH are presented in Figures 1 and 2. In Figure 1, the $N = 1 \rightarrow 0$ (upper) and $N = 2 \rightarrow 1$ (lower) transitions near 10 and 20 GHz, respectively, are displayed. The frequency breaks in the spectra allow all hyperfine lines to be shown. The Doppler doublets are designated by brackets above the spectral lines. Each transition $N+1 \rightarrow N$ is first split into spin-rotation doublets, which are separated by about 16 MHz, and indicated by *J*. For the $N = 1 \rightarrow 0$

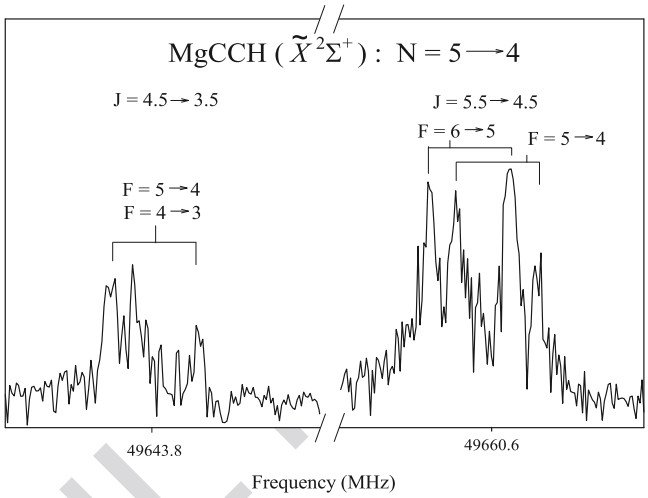


**Figure 2.** FTMmmW spectrum of MgCCH ($X^2\Sigma^+$) displaying the $N = 5 \rightarrow 4$ transition near 50 GHz. The spectrum is split into doublets by spin-rotation coupling, labelled by *J*, and then by hyperfine interactions, indicated by *F*. The hyperfine splitting is only resolved in the $J = 5.5 \rightarrow 4.5$ doublet. The Doppler doublets are indicated by brackets. There is one frequency breaks in the spectrum.

transition, the $J = 0.5 \rightarrow 0.5$ doublet is further split into two hyperfine lines, separated by ∼ 4 MHz, while the $J = 1.5 \rightarrow 0.5$ consists of three components with a similar splitting. Four frequency breaks in this spectrum show all five features. The $N = 2 \rightarrow 1$ transition consists of a total of four hyperfine components, two per spin-rotation doublet, which are separated by about ∼0.5 MHz in each doublet.

Figure 2 displays the $N = 5 \rightarrow 4$ transition of MgCCH measured near 49.6 GHz. Doppler doublets are again shown by brackets, and one frequency break is present in the data. Here, the hyperfine splitting is completely collapsed in the $J = 4.5 \rightarrow 3.5$ spin doublet and only barely resolved in the $J = 5.5 \rightarrow 4.5$ doublet with a separation of about 50 kHz.

The data were analyzed using an effective Hamiltonian consisting of rotational, spin-rotation and hyperfine interactions in a Hund's case b basis:

$$H_{eff} = H_{rot} + H_{sr} + H_{hf} \quad (8)$$

The FTMmmW data, which consisted of 21 measurements, were combined with the previous mm-wave data [13] for a global fit, using the non-linear least squares routine SPFIT [40]. The results of the analysis are shown in Table 2. As the table shows, the accuracy of the rotational constants *B* and *D* and the spin-rotation parameter $\gamma$ was improved by an order of magnitude in the combined fit and in *H* by a factor of ∼1000. Furthermore, the $\gamma_D$ constant was defined in the new fit, and the hydrogen hyperfine constants, $b_F$and *c*, were determined for

**Table 2.** Revised spectroscopic constants for MgCCH ($\tilde{X}^2\Sigma^+$).[a]

| Parameter | Combined fit | Previous mm-wave[b] |
|---|---|---|
| $B$ | 4965.33510(54) | 4965.3346(38) |
| $D$ | 0.00223267(44) | 0.0022324(20) |
| $H$ | $1.485349(10) \times 10^{-9}$ | $1.44(34) \times 10^{-9}$ |
| $\gamma$ | 16.6634(63) | 16.488 (45) |
| $\gamma_D$ | −0.0000318(79) | – |
| $b_F$ | 4.714(17) | – |
| $c$ | 1.835(39) | – |
| *rms* | 0.016 | 0.060 |

[a]In MHz. Values in parentheses are $3\sigma$ uncertainties.
[b]From ref [13].

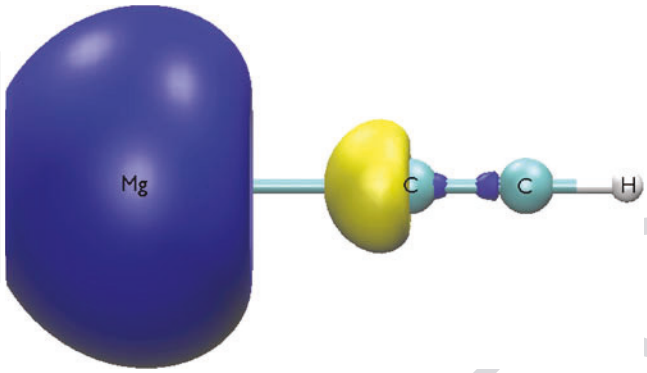


Colour online, B/W in print

**Figure 3.** 3D contour plot of the singly occupied $9A_1$ natural orbital of MgCCH ($X\,^2\Sigma^+$) at the aug-cc-pVTZ-DK CASSCF level of theory. An isovalue of 0.4 was used.

the first time. The rms of the combined fit was 16 kHz, as opposed to 60 kHz for the mm-wave data alone.

Perhaps the most interesting result of the analysis is the small values of the hyperfine constants, which are $b_F = 4.714(17)$ and $c = 1.835(39)$. The value of the Fermi contact parameter for the hydrogen atom is $b_F = 1420$ MHz [41], which indicates that 0.33% of the electron density of the unpaired electron is located on the H atom in MgCCH. Furthermore, the dipolar constant $c$, which is the angular term, indicates that there is little $p$ character to the orbital of the unpaired electron. In Figure 3, a contour plot of the $9A_1$ natural orbital is shown at the aug-cc-pVTZ-DK CASSCF level of theory. Indeed, both experimental and computational results suggest that the unpaired electron has predominantly nonbonding s orbital character on the magnesium centre.

### *Computations for neutral magnesium monoacetylide (MgCCH)*

The computed geometries and other spectroscopic constants for MgCCH are presented in Table 3. The additive corrections caused a slight shortening of bond lengths. Equilibrium geometries compare well between the CcC and CcC-F12 methods, agreeing to within 0.01 Å. From both composite approaches, the equilibrium bond distances are 2.04 Å for Mg-C, 1.22 Å for C–C, and 1.06 Å for C–H. Our $r_e$ values agree with those computed by Guo et al. [18] using B3LYP/6-31G* to produce bond lengths of 2.049 Å for the Mg-C bond, 1.224 Å for the C–C bond, and 1.069 Å for the C–H bond. Interestingly, the agreement between our coupled cluster results and DFT values from Guo is much better compared to results from the same work using the CASSCF/6-31G* level of theory, which provided respective bond lengths at 2.053, 1.242, and 1.058 Å.[10] The 'best' CcCRE approach gives a Mg-C $r_0$ bond distance of 2.0395 Å while CcCRE-F12 yields a bond distance of 2.0405 Å. Both the CcCRE and CcCRE-F12 composite methods agree to within 0.001 Å for the $r_0$(C–C) and $r_0$(C–H) values, 1.216 and 1.052 Å, respectively.

**Table 3.** Computed spectroscopic constants of the $^2\Sigma^+$ ground state of MgCCH.

| | CcC | CcCRE | CcC-F12 | CcCRE-F12 |
|---|---|---|---|---|
| $r_e(Mg-C)$ (Å) | 2.0382 | 2.0372 | 2.0393 | 2.0383 |
| $r_e(C-C)$ (Å) | 1.2221 | 1.2215 | 1.2223 | 1.2217 |
| $r_e(C-H)$ (Å) | 1.0645 | 1.0643 | 1.0646 | 1.0644 |
| $B_e$ ($cm^{-1}$) | 0.16521 | 0.1654 | 0.16507 | 0.1652 |
| $B_e$ (MHz) | 4952.888 | 4957.483 | 4948.815 | 4953.389 |
| $D_e$ (MHz) | 0.00199 | 0.00200 | 0.00199 | 0.00199 |
| $H_e$ (Hz) | −0.000574 | −0.000581 | −0.000572 | −0.000578 |
| $\omega_1$ ($cm^{-1}$) | 3428.1 | 3429.0 | 3429.2 | 3430.0 |
| $\omega_2$ ($cm^{-1}$) | 2007.3 | 2011.4 | 2007.5 | 2011.6 |
| $\omega_3$ ($cm^{-1}$) | 499.2 | 499.2 | 499.1 | 499.1 |
| $\omega_4$ ($cm^{-1}$) | 684.1 | 684.9 | 683.7 | 684.6 |
| $\omega_5$ ($cm^{-1}$) | 150.5 | 150.6 | 147.1 | 147.3 |
| $r_0(Mg-C)$ (Å) | 2.0404 | 2.0395 | 2.0414 | 2.0405 |
| $r_0(C-C)$ (Å) | 1.2167 | 1.2161 | 1.2167 | 1.2160 |
| $r_0(C-H)$ (Å) | 1.0526 | 1.0524 | 1.0526 | 1.0524 |
| $B_0$ (MHz) | 4962.232 | 4966.843 | 4959.119 | 4963.686 |
| $\alpha_1$ (MHz) | 8.321 | 8.302 | 8.290 | 8.268 |
| $\alpha_2$ (MHz) | 20.989 | 20.896 | 20.943 | 20.850 |
| $\alpha_3$ (MHz) | 0.822 | 0.810 | 0.946 | 0.950 |
| $\alpha_4$ (MHz) | 23.860 | 23.941 | 23.829 | 23.909 |
| $\alpha_5$ (MHz) | −36.752 | −36.738 | −37.781 | −37.762 |
| $\nu_1$ ($cm^{-1}$) | 3294.2 | 3294.9 | 3296.2 | 3297.0 |
| $\nu_2$ ($cm^{-1}$) | 1978.5 | 1982.7 | 1976.1 | 1980.3 |
| $\nu_3$ ($cm^{-1}$) | 487.5 | 487.4 | 501.6 | 501.5 |
| $\nu_4$ ($cm^{-1}$) | 659.0 | 659.0 | 667.8 | 667.9 |
| $\nu_5$ ($cm^{-1}$) | 139.5 | 138.9 | 145.2 | 144.6 |

Harmonic and fundamental vibrational frequencies for MgCCH are also provided in Table 3. The $\omega_2$ C–C stretching frequency exhibits the largest influence upon adding the Δ(CCSDT) and Δ(DK) additive corrections, blue-shifted from 2007 $cm^{-1}$ to 2011 $cm^{-1}$ for both CcCRE and CcCRE-F12 methods. While the scalar relativistic correction did not substantially change frequency values (Table S1), the CCSDT correction is responsible for this variation in $\omega_2$. The most significant difference in harmonic vibrational frequencies is in the $\omega_5$ bending mode, with CcCRE = 150.6 $cm^{-1}$ and CcCRE-F12 = 147.3 $cm^{-1}$. In order to better compare with previously reported theoretical harmonic vibrational frequencies of MgCCH, we have constructed composite values from the CCSD(T) computations of Woon [17]:

$\omega_{Woon} = w_{cc-pVTZ} + (\omega_{cc-pCVDZ} - \omega_{cc-pVDZ})$. The resulting harmonic frequencies are $\omega_1 = 3432\,cm^{-1}$, $\omega_2 = 1992\,cm^{-1}$, $\omega_3 = 495\,cm^{-1}$, $\omega_4 = 688\,cm^{-1}$, and $\omega_5 = 154\,cm^{-1}$. Except for the value of the C–C stretching frequency ($\omega_2$), there is reasonable agreement between the Woon composite values and the CcC/CcC-F12 values. The primary difference between CcC harmonic frequencies and the values from Woon is the better quality of the one-electron basis set in the present computations due to incorporation of CBS extrapolations or explicitly correlated wave functions. Thus, $\omega_2$ may be strongly basis set dependent. The CcCRE/CcCRE-F12 $\omega_5$ bending frequency (150.6/147.3 $cm^{-1}$, respectively) is the only computed observable that shows fair disagreement with experiment. Brewster et al. [13] provided 133 $cm^{-1}$ for $\omega_5$ using millimetre-wave spectroscopy, and dispersed fluorescence experiments from Corlett et al. determined a value of 143 $cm^{-1}$ [14]. However, there is remarkable agreement between the vibration-rotation constant $\alpha_5$ derived by experiment (–36.695 $cm^{-1}$) and theory (–36.738 $cm^{-1}$). Corlett also measured the $\omega_3$ stretch at 496 $cm^{-1}$, which is in excellent agreement with our calculated value of 499.1 $cm^{-1}$ using both CcCRE and CcCRE-F12.

We observe larger differences between CcCRE and CcCRE-F12 approaches for computed anharmonic frequencies compared to the tabulated harmonic frequencies. The maximum difference between harmonic frequencies computed with CcCRE and CcCRE-F12 is only 3.3 $cm^{-1}$ ($\omega_5$). The $\nu_1$ and $\nu_2$ fundamental frequencies corresponding to C–H and C–C stretches differ by a maximum of 2.4 $cm^{-1}$. The remaining stretching and bending modes undergo larger shifts, for example $\nu_3$ increases by +14.1 $cm^{-1}$ from 487.4 $cm^{-1}$ (CcCRE) to 501.5 $cm^{-1}$ (CcCRE-F12). Additionally, the $\nu_4$ and $\nu_5$ modes exhibit CcCRE→CcCRE-F12 shifts of +5.7 $cm^{-1}$ and +8.0 $cm^{-1}$, respectively.

Rotational constants for MgCCH were computed using coupled cluster-based QFF methodologies, which are known to provide accurate values for Mg-containing species [28,42]. Between the composite approaches, there is phenomenal agreement with the newly fit $B_0$ value of 4965.33510 (54) MHz; 4966.843 MHz at the CcCRE level of theory and 4963.686 MHz at the CcCRE-F12 level of theory. Higher-order centrifugal distortion constants are not greatly perturbed by vibrational anharmonicity. As a result, the trend of excellent agreement between theory and experiment continues for $D_e$ (experiment = 2.22 Hz, CcCRE = 2.00 Hz, CcCRE-F12 = 1.99 Hz). Unfortunately, computed sextic centrifugal distortion constants are the wrong sign and differ from experiment by a factor of ~3, but the difference in *H* constants does not quantitatively affect the purely *ab initio* line list constructed for MgCCH. Overall, the accuracy displayed here strengthens that the computational methods used are solid predictors of spectroscopic values not (yet) provided by experiment.

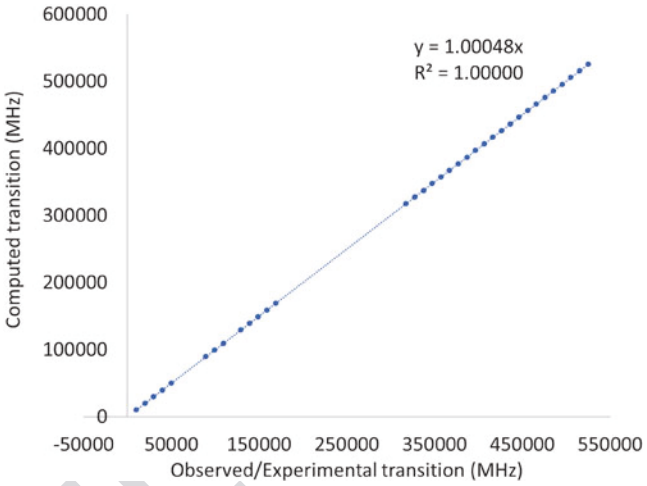


Colour online, B/W in print

**Figure 4.** Linear correlation between observed and computed (CcCRE) rotational transition frequencies for MgCCH ($X\,^2\Sigma^+$). The scale of the graph prevents visual distinction of spin-rotation components.

Using PGOPHER and the QFF-derived CcCRE rovibrational constants, a purely *ab initio* rotational Hamiltonian was constructed, and rotational lines for the neutral magnesium acetylide radical were calculated. In Figure 4, all known rotational lines of MgCCH from experiment (Cernicharo observations [4,11], previous [13] and current work from the Ziurys group) are compared against the CcCRE line list. The CcCRE-derived Hamiltonian captures spin-rotation doublets but does not include experimental or theoretical hyperfine constants. Thus, deviations to pure rotational results from the Ziurys group are calculated as the difference of the higher of two hyperfine doublets at a given rotational transition minus the lowest energy theoretical line. Rotational lines from the second survey of IRC +10216 carried out by Cernicharo and coauthors [11] are not given at high enough resolution to elucidate hyperfine doublets. Overall, 70 lines are included (Table S2), over four different ranges: (1) $N_\downarrow' = 0 \rightarrow N_\downarrow'' = 1$ to $N_\downarrow' = 5 \rightarrow N_\downarrow'' = 4$, (2) $N_\downarrow' = 9 \rightarrow N_\downarrow'' = 8$ to $N_\downarrow' = 11 \rightarrow N_\downarrow'' = 10$, (3) $N_\downarrow' = 13 \rightarrow N_\downarrow'' = 12$ to $N_\downarrow' = 17 \rightarrow N_\downarrow'' = 16$, and (4) $N_\downarrow' = 32 \rightarrow N_\downarrow'' = 31$ to $N_\downarrow' = 53 \rightarrow N_\downarrow'' = 52$. The difference between the observed and CcCRE values is small yet increases with increasing J-value as rotational energies are compounded. For example, the deviation between theory and experiment for $N_\downarrow' = 0 \rightarrow N_\downarrow'' = 1$, $J_\downarrow' = 3/2 \rightarrow J_\downarrow'' = 1/2$ is only – 1.02 MHz, while the deviation of – 254.3 MHz for $N_\downarrow' = 50 \rightarrow N_\downarrow'' = 49$, $J_\downarrow' = 50.5 \rightarrow J_\downarrow'' = 49.5$ is less predictive. A rigorous statistical

analysis of experiment versus theory is not pertinent due to the nonlinear dependence of rotational energies on $N$ or $J$ quantum numbers. However, the percent errors range from 0.010% to 0.056%. By constraining the trend line in Figure 4 to go through the origin, we obtain the correlation factor of *computed = experimental ∗ 1.000048* and use it to correct the theoretical line list for MgCCH. The deviation for $N' = 50 \rightarrow N'' = 49$, $J' = 50.5 \rightarrow J'' = 49.5$ using the 'semi-experimental' line list is reduced to ~ 21.2 MHz. Percent errors of the scaled line list range from a remarkable 0.0002% to 0.038%. If needed, the corrected theoretical lines can be used to assist in the identification of missing $J$ transitions of MgCCH, but the same correlation factor will also be applied to the $MgCCH^+$ cation to improve the quality of lines predicted by quantum chemistry. Computed and corrected lines are listed in Table S3.

### Computations for the magnesium monoacetylide cation ($MgCCH^+$)

Table 4 shows computed geometries as well as other spectroscopic properties of $MgCCH^+$ in its $^1\Sigma^+$ ground state. Like its neutral counterpart, additive corrections contributed no major shifts in the geometric parameters; that is, the corrections do not alter equilibrium bond lengths by more than 0.01 Å. The CcCRE method gave a Mg-C bond length of 1.928 Å; C–C bond length of 1.210 Å; and a C–H bond length of 1.058 Å and agrees with CcCRE-F12 values. Previous literature [17] using CCSD(T)/cc-pCVTZ puts the respective bond lengths at 1.93, 1.22, and 1.06 Å. Comparatively, the CcCRE-F12 method provides $r_0$ values of 1.9299, 1.2104, 1.0577 Å, fitting to a $B_0$ value of 5354.493 MHz. The presented geometric properties and vibrational data discussed below should reliably guide the laboratory and astrochemical characterisation of $MgCCH^+$.

Harmonic and fundamental vibrational frequencies for $MgCCH^+$ are also provided in Table 4. Additive corrections to CcC/CcC-F12 for small basis set CCDST and scalar relativity imparted similar shifts to spectroscopic constants of the cation (Table S3) as they did to the neutral MgCCH. Again, the greatest difference between CcCRE and CcCRE-F12 (+4.5 $cm^{-1}$) is observed in the $\omega_5$ bending mode. Harmonic vibrational frequencies computed with QFFs are within 10 $cm^{-1}$ of the values computed by Woon [17], with the exception of $\omega_2$ where CcCRE/CcCRE-F12 values are ~ 25 $cm^{-1}$ higher. Contrary to neutral MgCCH ground state, there is excellent agreement between both CcCRE and CcCRE-F12 anharmonic frequencies for $MgCCH^+$. We speculate the CcCRE and CcCRE-F12 QFFs are more similar for the cation because it is a closed-shell molecule, and neither MgCCH nor $MgCCH^+$ exhibit notable multireference character with $T_1/D_1$ diagnostics of 0.01/0.03 and 0.02/0.03, respectively. One exception in this consistency, however, is the $\nu_5$ bending mode with a CcCRE value of 142.9 $cm^{-1}$ and a CcCRE-F12 value of 137.8 $cm^{-1}$.

**Table 4.** Computed spectroscopic constants of the $^1\Sigma^+$ ground state of $MgCCH^+$ cation.

| | CcC | CcCRE | CcC-F12 | CcCRE-F12 |
|---|---|---|---|---|
| $r_e(Mg-C)$ (Å) | 1.9293 | 1.9279 | 1.9307 | 1.9292 |
| $r_e(C-C)$ (Å) | 1.2164 | 1.2157 | 1.2168 | 1.2161 |
| $r_e(C-H)$ (Å) | 1.0670 | 1.0667 | 1.0671 | 1.0669 |
| $B_e$ ($cm^{-1}$) | 0.17806 | 0.1783 | 0.17786 | 0.1781 |
| | 5338.128 | 5345.214 | 5332.198 | 5339.280 |
| $D_e$ (MHz) | 0.00171 | 0.00170 | 0.00171 | 0.00170 |
| $H_e$ (Hz) | −0.000216 | −0.000217 | −0.000224 | −0.000224 |
| $\omega_1$ ($cm^{-1}$) | 3414.3 | 3415.5 | 3414.7 | 3415.9 |
| $\omega_2$ ($cm^{-1}$) | 2045.5 | 2049.6 | 2044.9 | 2049.0 |
| $\omega_3$ ($cm^{-1}$) | 604.3 | 604.9 | 603.1 | 603.8 |
| $\omega_4$ ($cm^{-1}$) | 743.3 | 744.6 | 741.4 | 742.6 |
| $\omega_5$ ($cm^{-1}$) | 151.1 | 151.6 | 146.5 | 147.1 |
| $r_0(Mg-C)$ (Å) | 1.9301 | 1.9286 | 1.9314 | 1.9299 |
| $r_0(C-C)$ (Å) | 1.2110 | 1.2103 | 1.2110 | 1.2104 |
| $r_0(C-H)$ (Å) | 1.0578 | 1.0576 | 1.0579 | 1.0577 |
| $B_0$ (MHz) | 5352.368 | 5359.493 | 5347.383 | 5354.493 |
| $\alpha_1$ (MHz) | 9.227 | 9.212 | 9.180 | 9.163 |
| $\alpha_2$ (MHz) | 22.583 | 22.450 | 22.604 | 22.472 |
| $\alpha_3$ (MHz) | 0.782 | 0.746 | 1.083 | 1.046 |
| $\alpha_4$ (MHz) | 20.620 | 20.646 | 20.735 | 20.765 |
| $\alpha_5$ (MHz) | −41.237 | −41.179 | −42.528 | −42.458 |
| $\nu_1$ ($cm^{-1}$) | 3283.1 | 3284.2 | 3281.7 | 3282.9 |
| $\nu_2$ ($cm^{-1}$) | 2014.2 | 2018.5 | 2012.8 | 2017.2 |
| $\nu_3$ ($cm^{-1}$) | 606.7 | 607.3 | 605.4 | 606.0 |
| $\nu_4$ ($cm^{-1}$) | 717.4 | 718.2 | 718.9 | 719.6 |
| $\nu_5$ ($cm^{-1}$) | 144.3 | 142.9 | 139.4 | 137.8 |

Assuming the $J$-dependent offset of our purely theoretical rotational transitions for the parent neutral can translate to $MgCCH^+$, Table 5 contains an *ab initio* line list up to $J' = 26 \rightarrow J'' = 25$. With a closed shell ground state, the cation will not be affected by spin-rotation splitting. However, hyperfine splitting arising from the $I = \frac{1}{2}$; spin of the hydrogen atom will again split the experimental transitions into doublet but only by a small amount, as expected from nuclear spin-rotation interactions. As hyperfine constants have not been observed or determined computationally, these splittings are not accounted for in the CcCRE-derived line list. Despite some missing physics in our purely *ab initio* Hamiltonian, the reported pure rotational lines of the $MgCCH^+$ in the $^1\Sigma^+$ ground electronic state should be an accurate and reliable framework for spectroscopic and astronomical observations.

Finally, the ionisation potential (IP) of MgCCH was calculated using the composite methods reported throughout. Values corrected for the anharmonic zero-point energy are presented in Table 6. Accurate computation of the IP will provide a benchmark for future laser spectroscopy studies of MgCCH excited electronic states. Additive corrections have a miniscule effect on the ionisation potential, with Δ(CcCRE

**Table 5.** Rotational transitions of $MgCCH^+$ ($\tilde{X}^1\Sigma^+$) in MHz, predicted from CcCRE spectroscopic constants.

| $J'$ | | $J''$ | $\nu_{CcCRE}$ | $\nu_{scaled}$ |
|---|---|---|---|---|
| 1 | → | 0 | 10719 | 10714 |
| 2 | → | 1 | 21438 | 21428 |
| 3 | → | 2 | 32156 | 32141 |
| 4 | → | 3 | 42874 | 42854 |
| 5 | → | 4 | 53590 | 53564 |
| 6 | → | 5 | 64302 | 64271 |
| 7 | → | 6 | 75009 | 74973 |
| 8 | → | 7 | 85706 | 85664 |
| 9 | → | 8 | 96389 | 96343 |
| 10 | → | 9 | 107053 | 107001 |
| 11 | → | 10 | 117690 | 117633 |
| 12 | → | 11 | 128292 | 128230 |
| 13 | → | 12 | 138848 | 138781 |
| 14 | → | 13 | 149347 | 149275 |
| 15 | → | 14 | 159773 | 159696 |
| 16 | → | 15 | 170111 | 170029 |
| 17 | → | 16 | 180341 | 180254 |
| 18 | → | 17 | 190443 | 190351 |
| 19 | → | 18 | 200392 | 200295 |
| 20 | → | 19 | 210161 | 210060 |
| 21 | → | 20 | 219722 | 219616 |
| 22 | → | 21 | 229040 | 228930 |
| 23 | → | 22 | 238080 | 237966 |
| 24 | → | 23 | 246803 | 246684 |
| 25 | → | 24 | 255165 | 255042 |
| 26 | → | 25 | 263119 | 262992 |

Note: Scaled values obtained from the correlation of predicted versus observed lines of neutral ground state MgCCH are also listed.

**Table 6.** Composite ionisation potential of MgCCH in kcal/mol.

| | Ionisation potential (kcal/mol) |
|---|---|
| CcC | 166.26 |
| CcCR | 166.35 |
| CcCE | 166.31 |
| CcCRE | 166.41 |
| CcC-F12 | 168.09 |
| CcCR-F12 | 168.19 |
| CcCE-F12 | 168.15 |
| CcCRE-F12 | 168.25 |

Note: Note that all values are corrected using the anharmonic zero-point vibrational energy correction for neutral and cation provided in the SPECTRO output.

– CcC) = 0.15 kcal/mol. Surprisingly, the computed CcCRE and CcCRE-F12 IPs differ by 1.84 kcal/mol, suggesting differential one-electron basis set effects in either the neutral or cation species. Unfortunately, larger conventional and explicitly correlated basis sets than the ones used in this study have never been published. A deeper exploration of this minor mystery is outside the scope of current work.

## Conclusions

Quartic force fields obtained from quantum chemical methods used in this work again demonstrate utility in augmenting high-accuracy rovibrational experiments, and pave the way for detection of $MgCCH^+$ and other future interstellar organometallic molecules. Magnesium plays an important role in circumstellar chemistry. Of the known inventory of gas phase molecules, Mg is currently the most common metal found. MgCCH is one of the simplest of such known molecules, and a full spectroscopic characterisation has been needed to understand its chemical formation and to evaluate abundances through radiative transfer calculations. The new Fourier transform rotational measurements and accurate QFF computations of rotational and vibrational spectra have made progress in accomplishing these goals. The theoretical rotational constants $B_0$ and $\alpha_5$ obtained for MgCCH are in arguably perfect agreement with experiment, within 1.65 MHz and $< 0.07$ MHz of observed values, respectively. The $\Delta$(CCSDT) correction improved the accuracy of computed values for MgCCH while the scalar relativistic correction demonstrated little influence. Rotational line lists for MgCCH were computed purely from QFF-derived spectroscopic properties. A scale factor was determined for the neutral species, and then applied to the theoretical line list for $MgCCH^+$, a molecule which has no experimental data thus far and has eluded astronomical detection. As $MgCCH^+$ is a closed shell ion, the computed rotational constants for its ground state are expected to be as or more accurate than those computed for MgCCH, which should greatly assist in molecular characterisation. Thus, it expected that the QFF properties and predicted rotational lines of $MgCCH^+$ will be greatly useful for its experimental and astrochemical identification.

## Acknowledgements

The authors would like to express their heartfelt gratitude to Tim Lee, whose loss is felt deeply. Tim and LMZ were contemporaries during graduate school at University of California-Berkeley. Tim was RCF's postdoc advisor, and a friend and mentor to NJD. He will be missed, and his insights directly helped to push this research project forward.

RCF acknowledges funding from NASA Grant NNH22 ZHA004C, NSF Grant OIA-1757220, and the College of Liberal Arts from the University of Mississippi. LMZ and NJD acknowledge funding from NSF Grant CHE-2154121. JEB was partially supported by a NASA TN Space Grant Fellowship. The authors also thank Prof. José Cernicharo (Instituto de Física Fundamental-CSIC) for providing a table of fitted rotational line values, where previously we had derived the values from visual inspection of figures in reference [5].

## Disclosure statement

No potential conflict of interest was reported by the author(s). Q2

## Funding

This work was supported by National Aeronautics and Space Administration [grant number NNH22ZHA004C]; National

Science Foundation [grant number CHE-2154121]; Office of Integrative Activities [grant number OIA-1757220].

## ORCID

*Ryan C. Fortenberry* http://orcid.org/0000-0003-4716-8225

## References


[1] L.M. Ziurys, Ann. Rev. Phys. Chem. (in press).

[2] B.A. McGuire, Astrophys. J. Suppl. Ser. **239** (2), 17 (2018). doi:10.3847/1538-4365/aae5d2.

[3] J. Cernicharo and M. Guelin, Astron. Astrophys. **183**, L10 (1987); R.M. Humphreys, L.M. Ziurys, J.J. Bernal, M.S. Gordon, L.A. Helton, K. Ishibashi, T.J. Jones, A.M.S. Richards and W. Vlemmings, Astrophys. J. Lett. **874** (2), L26 (2019); L.N. Zack, D.T. Halfen and L.M. Ziurys, Astrophys. J. Lett. **733** (2), L36 (2011); R.L. Pulliam, C. Savage, M. Agúndez, J. Cernicharo, M. Guélin, and L.M. Ziurys, Astrophys. J. Lett. **725** (2), L181 (2010).

[4] J. Cernicharo, C. Cabezas, J.R. Pardo, M. Agúndez, O. Roncero, B. Tercero, N. Marcelino, M. Guélin, Y. Endo and P.D. Vicente, Astron. Astrophys. **672**, L13 (2023). doi:10.1051/0004-6361/202346467.

[5] J. Cernicharo, C. Cabezas, J.R. Pardo, M. Agúndez, C. Bermúdez, L. Velilla-Prieto, F. Tercero, J.A. López-Pérez, J.D. Gallego, J.P. Fonfría, G. Quintana-Lacaci, M. Guélin and Y. Endo, Astron. Astrophys. **630**, L2 (2019). doi:10.1051/0004-6361/201936372.

[6] L.M. Ziurys, A.J. Apponi, M. Guélin and J. Cernicharo, Astrophys. J. **445** (1 PART 2), L47 (1995). doi:10.1086/187886; J.R. Pardo, C. Cabezas, J.P. Fonfría, M. Agúndez, B. Tercero, P. de Vicente, M. Guélin and J. Cernicharo, Astron. Astrophys. **652**, L13 (2021).

[7] C. Cabezas, J. Cernicharo, J.L. Alonso, M. Agúndez, S. Mata, M. Guélin and I. Peña, Astrophys. J. **775**, 133 (2013). doi:10.1088/0004-637X/775/2/133; P.B. Changala, H. Gupta, J. Cernicharo, J.R. Pardo, M. Agúndez, C. Cabezas, B. Tercero, M. Guélin and M.C. McCarthy, Astrophys. J. **940**, L42 (2022); C. Cabezas, J.R. Pardo, M. Agúndez, B. Tercero, N. Marcelino, Y. Endo, P. de Vicente, M. Guélin and J. Cernicharo, Astron. Astrophys. **672**, L12 (2023).

[8] M. Guelin, J. Cernicharo, C. Kahane and J. Gomez-Gonzales, Astron. Astrophys. **157**, L17 (1986).

[9] J.L. Highberger, C. Savage, J.H. Bieging and L.M. Ziurys, Astrophys. J. **562** (2), 790 (2001). doi:10.1086/323231; J.L. Highberger and L.M. Ziurys, Astrophys. J. **597** (2), 1065 (2003).

[10] K.A. Kloska and R.C. Fortenberry, Mon. Not. R. Astron. Soc. **474** (2), 2055 (2017). doi:10.1093/mnras/stx2912; V. Adibekyan, N.C. Santos, P. Figueira, C. Dorn, S.G. Sousa, E. Delgado-Mena, G. Israelian, A.A. Hakobyan and C. Mordasini, A&A **581**, L2 (2015); V.Z. Adibekyan, N.C. Santos, S.G. Sousa, G. Israelian, E. Delgado Mena, J.I. González Hernández, M. Mayor, C. Lovis and S. Udry, A&A **543**, A89 (2012).

[11] M. Agúndez, J. Cernicharo and M. Guélin, A&A **570**, A45 (2014). doi:10.1051/0004-6361/201424542.

[12] M.A. Anderson and L.M. Ziurys, Astrophys. J. **439**, L25 (1995). doi:10.1086/187736.

[13] M.A. Brewster, A.J. Apponi, J. Xin and L.M. Ziurys, Chem. Phys. Lett. **310** (5), 411 (1999). doi:10.1016/S0009-2614(99)00816-7.

[14] G.K. Corlett, A.M. Little and A.M. Ellis, Chem. Phys. Lett. **249** (1), 53 (1996). doi:10.1016/0009-2614(95)01364-4.

[15] D.W. Tokaryk, A.G. Adam and W.S. Hopkins, J. Mol. Spectrosc. **230** (1), 54 (2005). doi:10.1016/j.jms.2004.10.008.

[16] C.A. Thompson and L. Andrews, J. Am. Chem. Soc. **118** (42), 10242 (1996). doi:10.1021/ja9616847.

[17] D.E. Woon, Astrophys. J. **456**, 602 (1996). doi:10.1086/176682.

[18] X. Guo, J. Zhang, J. Li, L. Jiang and J. Zhang, Chem. Phys. **360** (1), 27 (2009). doi:10.1016/j.chemphys.2009.04.004.

[19] S. Petrie, Mon. Not. R. Astron. Soc. **282** (3), 807 (1996). doi:10.1093/mnras/282.3.807.

[20] R.C. Fortenberry and T.J. Lee, in *Vibrational Dynamics of Molecules* (2022). pp. 235–295.

[21] I.M. Mills, in *Molecular Spectroscopy - Modern Research*, edited by K.N. Rao, C.W. Mathews (Academic Press, New York, 1972). pp. 115–140.

[22] J.K.G. Watson, in *Vibrational Spectra and Structure*, edited by J.R. During (Elsevier, Amsterdam, 1977). pp. 1–89.

[23] D. Papousek and M.R. Aliev, *Molecular Vibration-Rotation Spectra* (Elsevier, Amsterdam, 1982).

[24] X. Huang and T.J. Lee, J. Chem. Phys. **129** (4) (2008). doi:10.1063/1.2957488; R.C. Fortenberry, X. Huang, J.S. Francisco, T.D. Crawford and T.J. Lee, J. Chem. Phys. **135** (21) (2011); R.C. Fortenberry, X. Huang, T.D. Crawford and T.J. Lee, J. Phys. Chem. A **118** (34), 7034 (2014).

[25] X. Huang and T.J. Lee, J. Chem. Phys. **131** (10) (2009). doi:10.1063/1.3212560; R.C. Fortenberry, T.J. Lee and H.S.P. Müller, Mol. Astrophys. **1**, 13 (2015).

[26] Q. Cheng, R.C. Fortenberry and N.J. DeYonker, J. Chem. Phys. **147** (23), 234303 (2017). doi:10.1063/1.5006931.

[27] M.A. Burton, Q. Cheng, D.T. Halfen, J.H. Lane, N.J. Deyonker and L.M. Ziurys, J. Chem. Phys. **153** (3), 034304 (2020). doi:10.1063/5.0008746; R.C. Fortenberry and N.J. Deyonker, Acc. Chem. Res. **54** (2), 271 (2021).

[28] Q. Cheng, M.C. Washington, J.E. Burns, R.C. Fortenberry and N.J. DeYonker, Mon. Not. R. Astron. Soc. **498** (4), 5417 (2020). doi:10.1093/mnras/staa2646; D.A. Agbaglo, Q. Cheng, R.C. Fortenberry, J.F. Stanton and N.J. Deyonker, J. Phys. Chem. A **126** (26), 4132 (2022).

[29] M. Sun, A.J. Apponi and L.M. Ziurys, J. Chem. Phys. **130** (3, (2009).

[30] M. Sun, D.T. Halfen, J. Min, B. Harris, D.J. Clouthier and L.M. Ziurys, J. Chem. Phys. **133** (17, (2010).

[31] H.-J. Werner, P.J. Knowles, F.R. Manby, M. Schütz, P. Celani, G. Knizia, T. Korona, R. Lindh, A. Mitrushenkov, G. Rauhut, et al., *MOLPRO, Version 2018.2, a Package of Ab Initio Programs* (2018).

[32] K. Raghavachari, G.W. Trucks, J.A. Pople and M. Head-Gordon, Chem. Phys. Lett. **157** (6), 479 (1989). doi:10.1016/S0009-2614(89)87395-6.

[33] T.B. Adler, G. Knizia and H.-J. Werner, J. Chem. Phys. **127** (22, (2007). doi:10.1063/1.2817618.

[34] T.H. Dunning Jr., J. Chem. Phys. **90**, 1007 (1989). doi:10.1063/1.456153; B.P. Prascher, D.E. Woon, K.A. Peterson, T.H. Dunning and A.K. Wilson, Theor. Chem. Acc. **128** (1), 69 (2011).

[35] M. Douglas and N.M. Kroll, Ann. Phys. **82** (1), 89 (1974). doi:10.1016/0003-4916(74)90333-9.

[36] J. Grant Hill and K.A. Peterson, Phys. Chem. Chem. Phys. **12** (35), 10460 (2010). doi:10.1039/c0cp00020e; K.A. Peterson, T.B. Adler and H.-J. Werner, J. Chem. Phys. **128** (8) (2008).
[37] W.D. Allen and A.G. Császár, J Chem. Phys. **98** (4), 2983 (1993). doi:10.1063/1.464127.
[38] J.F. Gaw, A. Willets, W.H. Green and N.C. Handy, in *Advances in Molecular Vibrations and Collision Dynamics*, edited by J.M. Bowman, M.A. Ratner (JAI Press, Inc., Greenwich, CA, 1991). pp. 170–185.
[39] C.M. Western, J. Quant. Spectrosc. Radiat. Transf. **186**, 221 (2017). doi:10.1016/j.jqsrt.2016.04.010.
[40] H.M. Pickett, J. Mol. Spectrosc. **148** (2), 371 (1991). doi:10.1016/0022-2852(91)90393-O.
[41] P.B. Ayscough, *Electron Spin Resonance in Chemistry* (Methun, London, 1967).
[42] M.K. Bassett and R.C. Fortenberry, J. Mol. Spectrosc. **344** (61) (2018); C.Z. Palmer and R.C. Fortenberry, J. Phys. Chem. A **122** (35), 7079 (2018); D. Grosselin and R.C. Fortenberry, ACS Earth Space Chem. **6** (1), 18 (2022).